Nanoscale

PAPER

MRI-visible liposome nanovehicles for potential tumor-targeted delivery of multimodal therapies

Lili Ren,[a] Shizhen Chen,[a] Haidong Li,[a] Zhiying Zhang,[a] Chaohui Ye,[a] Maili Liu,[a] and Xin Zhou*[a]

Real-time diagnosis and monitoring of disease development, and therapeutic responses to treatment, are possible using theranostic magnetic resonance imaging (MRI). Here we report the synthesis of a multifunctional liposome, which contains Gd-DOTA (an MRI probe), paclitaxel and c(RGDyk) (a targeted peptide). This nanoparticle overcame the insolubility of paclitaxel, reduced the side effects of FDA-approved formulation of PTX-Cre (Taxol®) and improved the drug delivery efficiency to the tumor. c(RGDyk) modification greatly enhanced the cytotoxicity of the drug to tumor cells A549. The T_1 relaxivity in tumor cells treated with the targeted liposome formulation was increased 16-fold when compared with the non-targeted group. *In vivo*, the tumors in mice were visualized using T_1-weighted imaging after administration of the liposome. Also the tumor growth could be inhibited well after the treatment. Fluorescence images *in vitro* and *ex vivo* also showed the targeting effect of this liposome in tumor cells, indicating that this nanovehicle could limit the off-target side effects of anticancer drugs and contrast agents. These findings lay the foundations for the further tumor inhibition study and application of this delivery vehicle in cancer therapy settings.

Introduction

Liposomes, consisting of a 5-nm-thick lipid bilayer shell surrounding an aqueous core, are the most clinically established nanoscale systems used to deliver cytotoxic and antifungal drugs, genes, vaccines, as well as imaging agents.[1-12] Biocompatibility, biodegradability, reduced toxicity, and capacity for size and surface manipulations comprise the outstanding profile that liposomes offer over other delivery systems. As a drug carrier, liposomes have successfully encapsulated different therapeutic drugs, including doxorubicin,[12,13] platinum anticancer drugs,[5,14] cathepsin protease inhibitor,[3] irinotecan,[15] vinorelbine, parthenolide,[16] diclofenac sodium.[17] Paclitaxel, which is water insoluble and difficult to modification, can be successfully loaded in liposome to improve the therapy outcome.[18] Gd-chelates (Gd-DOTA/ Gd-DTPA) have been widely applied in clinical as its safety and positive magnetic resonance imaging (MRI) contrast.[19-22] As a contrast agent, Gd-chelate-encapsulated liposomes allowed significant contrast evaluation of drug efficacy in the tumor.[1,8,19-21]

Theranostic is a term that defines ongoing efforts to develop more specific, bespoke therapies for various diseases and combines these with diagnostic properties into a single pharmaceutical agent.[20,23,24] As the field of molecular imaging has emerged from the blending of molecular biology with medical imaging, liposomes are increasingly common for both therapeutic and diagnostic applications.[10,20,21] Diagnosis and therapy are traditionally regarded as two separate issues in medical care. To achieve an optimal curative effect for many diseases, especially in cancer, they have been combined mutually and synergistically. Theranostic liposomes provide a feasible approach to accurately locate the tumor tissues and monitor the drug behaviors and therapeutic responses to individual treatments.[1,3,8,19,25]

To further decrease the side effects and improve the accumulation of the drug and contrast agents in the tumor, a group selective for cancer cells is needed.[4-12] Integrin, overexpressed in many solid tumor cells, has a direct effect in preventing apoptosis in cancer cells and mediating proangiogenic interactions between endothelial cells and the extracellular matrix.[21,26-29] Peptides with arginine-glycine-aspartic acid (RGD) sequences are known to bind to integrin receptors with high affinity. Probes with RGD peptides have been used to image $\alpha_v\beta_3$ integrin receptor expression and related objects by fluorescence, MRI, PET or other techniques.[17,27,30] Cyclic targeted peptide, c(RGDyK), has a higher binding affinity and specificity when compared with linear peptides or multimers of the RGD peptide.[18,31–34] As

illustrated in Fig. 1, nanoparticles with RGD peptides can be internalized into tumor cells and release substances to treat cancer and enhance the tumor signal.[5,9,27,31,35]

The work presented here addresses the development of an effective approach for the preparation of a theranostic liposome, which contains paclitaxel in the biolayer for cancer drug treatment, a targeted group, c(RGDyK), and Gd-DOTA as T_1 contrast agent for MRI-visible enhancement for non-small lung cancer cell, A549 ($\alpha_v\beta_3$ integrin positive cell[27-29]). Liposomes were also labeled with rhodamine for detection by fluorescence imaging. The behavior of this theranostic nanoprobe was detected *in vitro* and *in vivo*. These bifunctional liposomes, possessing both MRI-visible and therapeutic potential, may hold promise as theranostic agents for multimodal nanomedicine, owing to properties including high sensitivity, deep tissue penetration and good anticancer efficiency.

Experimental

Chemicals

1,2-distearoyl-*sn*-glycero-3-phosphocholine (DSPC), 1,2-distearoyl-*sn*-glycero-3- phosphoglycerol sodium salt (DSPG-Na) and N-(Carbonyl-methoxypolyethyleneglycol-2000)-1,2-distearoyl-*sn*-glycero-3-phosphoethanolamine, sodium salt (MPEG-2000-DSPE) were purchased from Corden Pharma. N-(carboxy-polyethyleneglycol-2000)-1,2-distearoyl-*sn*-glycero-3-phosphoethanolamine, ammonium salt (COOH-PEG2000-DSPE) was purchased from NANOCS. 1,2-dimyristoyl-*sn*-glycero-3-phosphoethanolamine-N-(lissamine rhodamine B sulfonyl, ammonium salt (Rhod-DMPE) was purchased from Avanti Polar lipids. DOTA was purchased from Strem Chemicals. $GdCl_3$ was from Sigma–Aldrich. c(RGDyK) was obtained from GL Bioche. Paclitaxel was from Shyuanye. All other reagents were of analytical grade.

Preparation of paclitaxel-contrast agent-loaded and fluorescence-labeled liposomes

The liposome composed of DSPC, DSPG, and MPEG-2000-DSPE at 7:2:1 (mol) was prepared by a thin film hydration method, followed by membrane extrusion.[5,12,15,16] Briefly, 15 mg of lipids were dissolved in 1 ml chloroform/methanol/water (1:1:0.3, v/v/v) and dried under a vacuum to form a film. The resulting lipid film was then placed under high vacuum overnight and hydrated with PBS (pH 7.4) by sonication in water bath for 10 min. The blank liposome was obtained.

For PTX-contrast agent-loaded liposome (Gd-PTX-L), PTX was added to the lipid solution at a molar ratio of 1:30 (drug:lipid). The lipid film was formed by evaporation using rotary evaporator. The film was then hydrated with 1 ml of an aqueous solution of 150 mM DOTA/100 mM $GdCl_3$ (pH3.5) to form multilamellar vesicles. These vesicles were sonicated for 10 min and subsequently extruded 10 times through polycarbonate filters, 0.2 μm pore size, by an Avanti mini-extruder. Non-encapsulated PTX was removed by centrifuging for 10 min at 2000 rpm. The exterior buffer of the liposome

was exchanged by PBS (pH 7.4) via dialysis (10kD) for 4 h.[1,4,36]

To form the targeted liposome (RGD-Gd-PTX-L), the peptide-lipid conjugate c(RGDyK)-PEG2000-DSPE was synthesized.[37,38] COOH-PEG2000-DSPE was dissolved in PBS buffer. Appropriate amounts of N-hydroxysuccinimide (NHS) and 1-(3-dimethylaminopropyl)-3-ethyl carbodiimide hydrochloride (EDCI) were added to the solution. After incubation at room temperature for 30 min, c(RGDyK) was added and incubated for 10 h. Excess unreacted peptide was removed by dialysis (2000D). The conjugate was then lyophilized for the subsequent procedures. The molar ratio was 7:2:1:0.5 of DSPC, DSPG, MPEG-2000-DSPE and c(RGDyK)-PEG2000-DSPE. Targeted liposome preparation was the same as that of Gd-PTX-L.

Rhodamine-labeled liposome (Rh-L) was composed of DSPC, DSPG, MPEG-2000-DSPE and Rhod-DMPE at the molar ratio of 7:2:1:0.2. Rhod-DMPE was dissolved in the organic phase. The fluorescent liposome was prepared by the same method as above.[1,6,37] The whole process was protected from light.

The resulting liposomes were characterized using dynamic light scattering (DLS) with a zetasizer nano ZS (Malvern, England) for hydrodynamic diameter and zeta potential, and transmission electron microscopy (TEM) by Tecnai G20 (FEI, USA).

Quantification of encapsulated PTX and Gd

The content of PTX incorporated into liposomes was detected by HPLC (Agilent, USA).The liposomes were diluted by adding water and acetonitrile to a total volume of 0.5 ml. PTX was extracted by adding 4.0 ml of tert-butyl methyl ether and mixing for 30 s. The mixture was centrifuged for 15 min at 300 $\times$ g, after which 3 ml of the organic layer was transferred and evaporated. The residue was dissolved with 100 μl of 7/3 acetonitrile/water mixture. 50 μl of this solution was injected into a C_{18} column guard. The flow rate was 1.0 ml/min; the detection wavelength was set at 227 nm. The drug concentration was calculated from standard curves. The assay was linear over the concentration range from 1 μg to 500 μg.[4,39]

The Gd content of the liposomes was determined by ICP-MS (Thermo, USA).[14] A sample volume of 0.25 ml was diluted with 0.5 ml water. After addition of 1.5 ml HNO_3, the sample was heated to approximately 100 ℃ for 30 min. The sample was then further diluted to 50 ml with water.[40] Calibration was done with a Gd ICP standard solution. The encapsulation efficiency was calculated according to equation 1, in which $PTX(Gd)_{final}$ is the content of PTX or Gd in the liposome and $PTX(Gd)_{total}$ is the original content added to the lipid.

$$\text{encapsulation efficiency}(\%) = PTX(Gd)_{final} \ / \ PTX(Gd)_{total} \times 100\% \text{......(1)}$$

Physical stability of liposomes

The physical stability of RGD-Gd-PTX-L were evaluated in the storage condition (in PBS) at 4 ℃ and in fetal bovine serum (liposome:serum=1:2, v/v) at 37 ℃. Certain amounts of samples were taken from the pool at different times. The samples were

centrifuged for 15 min at 300 × g. The following PTX extraction and detection were as the same as the content of PTX above. The released drug can be calculated compared to the original content of PTX in the liposome.[39]

Fluorescence microscopy studies of the targeted liposomes

Non-small lung cancer cell A549 and human normal lung fibroblast cell WI-38 (1×10^5 cells) were seeded on cover slips placed in a cell culture dish and cultured in IMDM (Iscove's Modified Dulbecco's Medium, Boster, China) and MEM (Minimum Essential Medium, Boster, China) respectively, supplemented with 10% fetal bovine serum (Boster, China), 100 U/ml penicillin and streptomycin (Boster, China) in a humidified air with 5% CO_2 at 37 ℃. The regular culture mediums were removed when the cell confluence reached to 30%–40%. IMDM and MEM medium containing the rhodamine-labeled liposome was added. After 4 h of incubation at 37 ℃, the cells were incubated with DAPI for 5 min. All cells were washed at least three times with PBS. The fluorescence images were taken by Confocal Laser Scanning Microscope (CLSM, Nikon, Japan).[4,5]

In vitro cytotoxicity assays

Approximately 1×10^4 cells were seeded per well in 96-well plates and cultured for 24 h. RGD-Gd-PTX-L, Gd-PTX-L, blank liposomes and PTX (dissolved in Cremophor/ehanol, 50:50, v/v) were diluted in IMDM/MEM medium and added to the wells. After 4 h of incubation, the cells were then cultured in regular culture medium for 2 days. MTT was added to the culture medium at a concentration of 0.5 mg/ml during the last 4 h of the culture. The medium was carefully removed and 200 μl DMSO was added per well. The optical density at 490 nm for each well was measured by an ELISA plate reader (Molecular Devices, USA).[5,34,41] The 50% inhibitory concentration (IC50) was graphically calculated from concentration-effect curves, taking the optical density of control well as 100%.

Cellular uptake study

The cells (1×10^6 cells) were cultured in 25-ml cell culture flasks until >90% confluence was reached. After 4 h of incubation with RGD-Gd-PTX-L and Gd-PTX-L (containing 20 μg paclitaxel each), the cells were harvested using 1% triton to destroy any cell pellets.[41] The extraction and detection methods of PTX were as the same as detailed for the quantification of PTX. The cellular uptake efficiency was calculated as equation 2, in which PTX_{cell} is the content of PTX inside of the cell and PTX_{lipo} is the content inside of the liposome.

$$\text{cellular uptake efficiency (\%)} = PTX_{cell} \ / \ PTX_{lipo} \times 100\% \ ...... (2)$$

In vitro MR contrast properties of the liposomes

The cell culture process was as the same as cellular uptake study. When the cells confluence was greater than 90%, the targeted liposome (RGD-Gd-PTX-L) and control group (Gd-PTX-L) were diluted with IMDM/MEM to differing concentrations of Gd and then added to the flasks. After 4 h of incubation, cells were washed at least three times to remove any unbound liposomes and harvested with 500 μl H_2O/D_2O (2:98, v/v).[41]

The MR contrast effect of this liposome was examined by measuring the proton longitudinal relaxation time (T_1) of the cell solution, which refers to the longitudinal relaxation rate ($1/T_1$) in the presence of paramagnetic substances. All the samples were detected by 500 MHz NMR analyzer (Bruker, USA) with a standard inversion-recovery pulse sequence. Furthermore, 250 μl of the samples added to 96-well plate were imaged using a 7T MRI scanner with a spin-echo method (TR=500 ms; TE=11 ms; FOV=8×8 cm; 10 mm slice thickness) (Bruker, USA).[1,14,40]

In vivo MR contrast properties of the liposomes

BALB/c male nude mice (aged 5–6 weeks, approx. 20 g) were inoculated subcutaneously on the legs with A549 cells (1×10^6 cells in 250 μl PBS) and examined using MRI 3 weeks after inoculation. 7T MRI monitored the liposomes, which were gathering in tumor-bearing mice, by repeat scanning prior to treatment (for baseline evaluation) and post-treatment. Tumor-bearing mice were oriented in the prone position. The mice were initially anesthetized with 3% isoflurane and then 1% isoflurane using a gas controller (Matrx, USA). The respiratory cycle was monitored using a pneumatic pillow. T_1 was measured using a saturation-recovery technique, involving acquisition of T_1-weighted MR images before and after administration of the liposome via the tail vein, using a spin echo technique (TE =11 ms; TR = 120, 150, 180, 200, 300, 500, 800, 1200, 2000, 3000, 5000 ms; 1 mm slice thickness; 22 min data acquisition; RARE factor=1; matrix size=256×256, FOV=4×4 cm.).[1,14] Image analysis was performed by ParaVision 5.0.

For the *ex vivo* study, rhodamine-labeled liposome (Rh-RGD-Gd-PTX-L) was injected intravenously (i.v.) to the A549-grafted mouse model. After 1 h administration, the tumor was resected, fixed in 10% paraformaldehyde overnight, dehydrated by 30% sucrose and molded with paraffin or frozen for section. The sections were cut to a 20-μm thickness and stained with DAPI for fluorescence imaging by CLSM. The sections were cut with 10-μm and stained with haematoxylin and eosin for histological analysis.[3]

In vivo tumor inhibition effect

Tumor inhibition effect of RGD-Gd-PTX-L on tumor was evaluated by 7T MRI scanner. The fixation and anesthesia process were as the same as above. 200 μl liposome was injected via tail vein. The control group was injected with the same volume of saline. The liposome and saline were injected on days 0, 2, 4, 7, 10, 14 and 16. The MRIs were taken on day 0, 10 and 23 with the same parameters as before. When taking the MRIs of the control group, the same amount of RGD-Gd-L was applied. T_1-weighted MRIs were obtained 1 h after the administration of the contrast agent-loaded liposome. Image analysis was performed by ParaVision 5.0. Regions of interest

were identified using a mouse atlas of anatomy. The tumor volume was estimated as the sum of the tumor volume of all slices.[1,4]

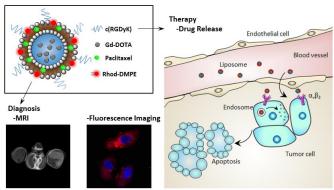## Results and discussion

Characterizations

Fig.1 Schematic of the structure of the multifunctional liposome and the application of this liposome in theranostics. The nanoprobes can be internalized and activated by $\alpha_v\beta_3$-madiated endocytosis in tumor cells. The drug and contrast agent can be released after the destabilization of the endosome provoked by the liposome, thus realizing targeted imaging and tumor therapy.[5,9,27,31,35]

Table 1 Formulation parameters. All the data was the mean±standard deviation (SD), n=3.

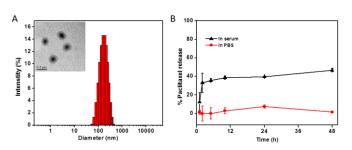| Group	Diameter (nm)	Zeta potential (mv)
RGD-Gd-PTX-L	161.7±5.5	−7.97±3.99
Blank L	141.1±8.7	−5.79±1.27
	Concentration	Entrapment efficiency (%)
Gd	3.28±0.26 mM	14.36±3.85
PTX	0.12±0.04 mg/ml	71.10±4.73

Fig.2 (A) DLS measurement of the corresponding liposome showing the distribution of diameters and the size (diameter=162.2 nm). The insert: image of RGD-Gd-PTX-L by TEM shows the round-shape of the liposome. (B) *In vitro* release of paclitaxel from RGD-Gd-PTX-L in storage conditions at 4 ℃ or in serum at 37 ℃. Data were presented as mean±SD, n=3.

The structure of the multifunctional liposome is illustrated in Fig. 1. Liposomes are composed of the lipid molecules that self-assemble into a hollow double-layer sphere, into which PTX and Gd-DOTA are inserted. Targeted ligand c(RGDyK) is covalently conjugated to the liposome. This liposome can be

delivered to tumor site and release anticancer drugs and contrast agents *in vivo*. TEM images provide evidence for the round shape of these particles with mean diameters around 162 nm, as detected by DLS (Fig. 2A). The drug release was 1.5% after 2 days storing in PBS at 4 ℃ and 46.84% in serum at 37 ℃ (Fig. 2B), indicating the good physically stability of RGD-Gd-PTX-L in storage conditions and relatively slow drug release in serum. The high drug release rate in serum may relate to the high temperature and serum protein. High temperature may speed up the release of drug from liposome. Also the liposome structure would be changed by exposure to serum proteins.[9,37,39] The formulation parameters are listed in Table 1. RGD-Gd-PTX-L was 161.7±5.5 nm. Approximately 14.36±3.85% of Gd-DOTA was loaded into the targeted liposome. The loading efficiency of PTX was 71.10±4.73%.

Tumor targeting by fluorescence analysis

To investigate the tumor targeting of c(RGDyk) modified liposome, lung cancer cell A549 and normal lung cell WI-38 were incubated with rhodamine-labeled RGD-Gd-PTX-L and Gd-PTX-L. Fig. 3A showed the fluorescence micrographs of different groups. For A549 cells, the red fluorescence (attributed to rhodamine) intensity in RGD-Gd-PTX-L-bound cells was distinguishably higher than that of Gd-PTX-L-bound cells. For WI-38 cells, the fluorescence intensity was quite low. The differences between groups of RGD-Gd-PTX-L and Gd-PTX-L were obvious. Also A549 cell absorption of liposomes could be clearly seen in different slices (Fig. 3B). Most liposomes were located in the cytoplasm. Co-localization of red and blue showed that a few liposomes reached the nucleus. This phenomena demonstrated receptor mediated endocytosis when the integrin receptor on the tumor cell specifically recognized the targeted liposome.[5,27,31] Overall, the fluorescence intensity was much higher in A549 cells compared to WI-38 cells. Thus this drug delivery system may decrease the side effects of PTX and improve the drug efficiency.[5]
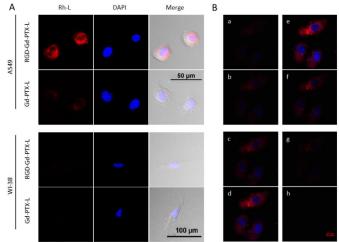

Fig.3 (A) Binding of rhodamine labeled liposomes (red) in tumor cell A549 and normal cell WI-38 by confocal laser scanning microscopy. A549 and WI-38 were treated with Rh-RGD-Gd-PTX-L and Rh-Gd-PTX-L at the PTX concentration of 1 μg/ml for 4 h at 37 ℃. Cell nucleus was stained with

DAPI (blue). (B) Internalization of targeted liposome (red) in A549 cells. Eight slices of fluorescence images from the top to the bottom (a to h) of the cells were shown using the Z-stack scan mode (step=2 μm).

Cytotoxicity of liposomes and cellular uptake of PTX

To explore whether the specific delivery of the therapeutic cargo to the tumor cells results in improved drug action, cell-killing ability of different groups of liposome was evaluated by MTT assay. Blank liposomes had no significant effect on either cell lines (the data weren't showed here). The results demonstrated dose-dependent toxicity on A549 and WI-38 cells (Fig. 4A). Integrin is highly expressed in many cancer cells, RGD peptides can target integrin and induce apoptosis.[26] When the concentration of PTX was 16 μg/ml, the viability of A549 cells was approximately 38% and 75.4% for targeted and control group, respectively. The cytotoxic effect of RGD-Gd-PTX-L and Gd-PTX-L on WI-38 was relatively low, even when the concentration of PTX was 16 μg/ml (the cell viability was about 97.33% and 98.64%, respectively). Apoptotic response in A549 cells was much stronger than in WI-38 cells. RGD-Gd-PTX-L resulted in significantly higher toxicity than Gd-PTX-L for A549 cells, suggesting that c(RGDyk)-modified liposome decreased cell viability, resulting in a lower IC50 (15 μg/ml and 35 μg/ml of RGD-Gd-PTX-L and Gd-PTX-L, respectively in A549 cells).
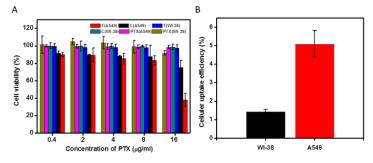

Fig.4 (A) Liposomal PTX drug efficacies in A549 and WI-38. PTX loaded liposomes and PTX were added into both cell lines at the concentrations of 0.4, 2, 4, 8 and 16 μg/ml. The resulting cytotoxicity was determined as a percentage of viable cells. RGD-Gd-PTX-L (T) and Gd-PTX-L (C) were targeted and control liposome respectively. Data were presented as mean±SD, n≥3. (B) Cellular uptake of RGD-Gd-PTX-L by A549 and WI-38. Data were presented as mean±SD, n=3.

In order to ascertain the exact amount of PTX internalized by A549 and WI-38 cells, PTX was extracted and then detected by HPLC. RGD-Gd-PTX-L showed an approximate 3.6-fold increase in uptake by A549 cells when compared to WI-38 cells under the same conditions (Fig. 4B). These results confirmed that this novel integrin-targeted-PTX-loaded liposome had low, non-specific toxicity and a more efficient antitumor effect than non-targeted equivalents.

In vitro MR contrast enhancement of the targeted liposomes

The MR contrast properties of RGD-Gd-PTX-L were evaluated *in vitro* using A549 and WI-38 cell lines. The longitudinal relaxation times (T_1) were measured using different

concentrations of RGD-Gd-PTX-L and Gd-PTX-L. The baseline of longitudinal relaxation rates ($1/T_1$) for the pre-treatment tumor cells was 0.13 ± 0.01 s^{-1} at 500 MHz and then increased significantly after incubation with Gd-DOTA-loaded liposomes (4.03 ± 0.04 s^{-1} and 2.95 ± 0.03 s^{-1} for targeted and control groups, respectively, at Gd concentration of 0.6 μM) (Fig. 5A). $1/T_1$ of A549 cells decreased (for example, 3.39 ± 0.13 s^{-1} for the targeted group) when the concentration of Gd was increased to 1 μM. This might be related to the alteration of cell structure and function when treated with relatively high drug concentrations. The largest $1/T_1$ of A549 cells incubated with targeted liposome increased more than 30 times compared to that of A549 cells treated with non-targeted liposomes. As for WI-38 cells, $1/T_1$ was increased gradually with the increase of the liposome concentration. $1/T_1$ was 0.44 ± 0.02 s^{-1} and 0.38 ± 0.01 s^{-1} for targeted and control group, respectively, when Gd concentration was 1 μM. There was no significant difference in $1/T_1$ between the targeted and control group in WI-38 cells. Longitudinal relaxation enhancement of A549 cells was much larger than WI-38 cells, indicating the site-specific accumulation of liposomes in cancer cells.[31] The more liposomes were internalized into cells the larger the longitudinal relaxation rate, and the greater the enhancement of MRI signal. The $1/T_1$ obtained by 7T showed similar results as above (the data weren't showed here).

The longitudinal relaxation times of tumor cells incubated with targeted liposomes for different periods was also investigated (Fig. 5B). $1/T_1$ increased gradually when the incubation time was longer, peaking on day 2 (4.66 ± 0.23 s^{-1}). It then dropped greatly in day 3 (0.18 ± 0.01 s^{-1}). T_1 relaxivity improved with the increasing Gd-DOTA, and then decreased when cell apoptosis started to occur. Thus, it is possible that the drug effect and tumor variation could be detected *in vivo* by MRI.
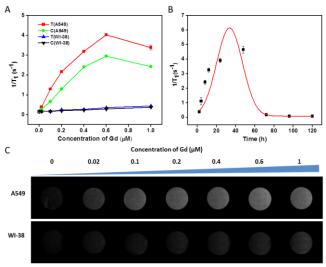

Fig.5 MR contrast properties of targeted liposomes. (A) Longitudinal relaxation rates ($1/T_1$) of A549 and WI-38 incubated with Gd-DOTA-loaded liposomes detected by 500 MHz NMR analyzer. The concentrations of Gd were 1, 0.6, 0.4, 0.2, 0.1 and 0.02 μM respectively. T represented RGD-Gd-PTX-L; C was Gd-PTX-L. (B) $1/T_1$ of A549 incubated with RGD-Gd-PTX-

L at different time (PTX, 26 μg/ml; Gd, 1 μM) detected by 500 MHz NMR analyzer. (C) T_1-weighted MR images of A549 and WI-38 incubated with RGD-Gd-PTX-L at different concentrations corresponding to (A) detected by 7T scanner. Data were presented as mean±SD, n=3.

T_1 variation of tumor and normal cells incubated with liposomes could be visualized, as shown in Fig. 5C. The T_1 signal was improved gradually with the increasing concentration of Gd in both cell lines, with the exception of A549 cells when Gd was 1 μM (the signal decreased). Briefly, the signal in A549 cells was much higher than found in WI-38 cells under the same conditions. Furthermore, the signal from the targeted group was much higher than that of the control group. Compared to normal cell (WI-38), the tumor cells (A549) absorbed more liposome. This can be possibly by accounted for by the greater number of receptors on the tumor cell surface and/or the different behaviors of the cell lines.[5]

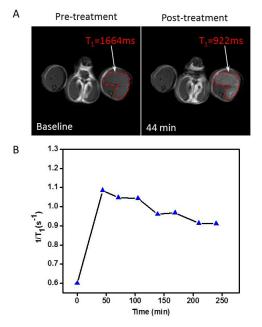**Targeted liposome as MRI-visible drug delivery system *in vivo***

Fig.6 MRI analysis of the tumors before and after treatment with targeted liposomes. (A) T_1-weighted MR images of a mouse before and after the treatment with RGD-Gd-PTX-L. The tumor boundary is demarcated by the red dotted line. The tumor volume was approximately 5×3 mm. (B) Longitudinal relaxation rates ($1/T_1$) variation of the tumor with the time after administration of the targeted liposome.

As shown in Fig. 6A, T_1 relaxation was significantly accelerated in the tumor after i.v. injection of liposome at a Gd concentration of 8 μM/kg. The T_1 baseline for the pre-treatment tumor was 1664 ms, which then decreased 44 min after administration of targeted liposome (922 ms). Not only the rim, but also the core of the tumor turned bright. The decrease percent of T_1 was 44.59% and 43.61% respectively after 44 min or 1 h administration of the liposome. The contrast enhancement was much higher than some reaserch[1,32]. The T_1 relaxation enhancement was maintained for more than 4 h (Fig. 6B) then returned to original levels after 1 day (T_1 was 1600 ms

at 24 h). No significant acute toxicity was recorded in the mouse during and after the test and the liposomal formulation of the PTX overcame the poor solubility of this drug, reducing dose-related side effects.[4,18,39,42−44] Also the contrast enhancement was relatively high for a long period, which may be related to the enhanced permeability and retention effect,[14,18] and the longer blood circulation time of the liposome provided by PEG-lipid.[1,18,39] Collectively, this particle has improved tumor targeting ability via i.v. administration, and monitoring by MRI.
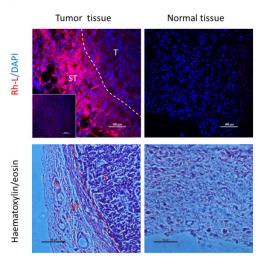

Fig.7 *Ex vivo* detection of fluorescent-targeted liposome in tumor. Representative fluorescent and hematoxylin & eosin staining images of tumor and normal tissue after injection of Rh-RGD-Gd-PTX-L (red). Insert: image of inside tumor. Stromal (ST) and tumor (T) compartment of the tumor tissue are demarcated by the dotted line. Tumor volume was approximately 3.5×3 mm.

To further study the targeting ability of the liposome *in vivo*, rhodamine-labeled liposome was injected into the cancer cell transplanted mouse. Fluorescence images were taken by CLSM after tissue sections were prepared. The liposome was successfully delivered to the tumor site (Fig. 7), not only inside the tumor (Fig. 7, inset), but also in the stroma whereas the normal cell absorbed very little liposome. Combined with the tumor T_1-weighted MR images, the fluorescence results also showed the targeting effect of liposomes to the tumor site *in vivo*. Most importantly, the liposome could be identified in the tumor microenvironments. It is known that the tumor stroma is important for tumor progression.[3,45] This is promising for early cancer or tumor metastasis control.

The antitumor efficiency of this multifunctional liposome could be monitored by T_1-weighted MRIs (Fig. 8). Compared with the control group, the representative tumor images showed apparently tumor growth inhibition by RGD-Gd-PTX-L, especially at day 10 after the first week of intense drug administration. The tumor volumes of the liposome and saline groups were 8 and 9 mm³ before the treatment, and 17 and 30 mm³ after the treatment period, respectively. These results showed the potential of the liposomes in effective lung cancer treatment. Based on the preliminary studies, these liposomes could be involved in further applications, such as detecting and

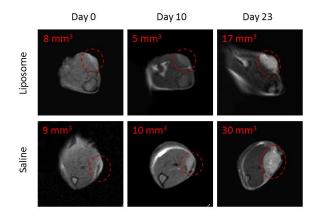monitoring the tumor development and treatment effect by MRI, potentially in other cancer models.

Fig.8 *In vivo* antitumor efficiency of RGD-Gd-PTX-L on A549 implanted mice model assessed by MRI. Tumors were marked by the red dotted line. The tumor volumes were 8, 5, 17 mm^3 for liposome group, and 9, 10, 30 mm^3 for control group respectively, at different time points.

Conclusions

In conclusion, lipophilic paclitaxel and hydrophilic Gd-DOTA were successfully assembled into one liposome. c(RGDyk)-modified liposomes can effectively target A549 non-small lung cancer cells *in vitro* and *in vivo*. This delivery system could provide a minimally invasive and real-time MRI strategy with improved sensitivity over non-targeted delivery vehicles. Furthermore, the targeted liposome can effectively target to tumor and tumor microenvironments detectable by a fluorescent technique. The therapeutic effect of this multifunctional liposome provides an exciting avenue to pursue the further application in lung cancer. More generally, integrin is overexpressed in many solid tumor cells and an important target for regulating cancer progression. Therefore, such a peptide-modified liposome may be applicable as carriers in other cancer-related diagnoses and treatment settings.

Acknowledgments

Notes and references

a Address here. ªKey Laboratory of Magnetic Resonance in Biological Systems, State Key Laboratory of Magnetic Resonance and Atomic and Molecular Physics, National Center for Magnetic Resonance in Wuhan, Wuhan Institute of Physics and Mathematics, Chinese Academy of Sciences, Wuhan 430071, China
*Phone: 86-027-8719-8802. Fax: 86-27-8719-9291.
 E-mail address: xinzhou@wipm.ac.cn.

1 T. Tagami, W.D. Foltz, M.J. Ernsting, C.M. Lee, I.F. Tannock, J.P. May and S.D Li, *Biomaterials,* 2011, **32**, 6570-6578.
2 Y. Chen, A. Bose and G.D. Bothun, *ACS NANO*, 2010, **4**, 3215-3221.
3 G. Mikhaylov, U. Mikac, A.A. Magaeva, V.I. Itin, E.P. Naiden, I. Psakhye, L. Babes, T. Reinheckel, C. Peters, R. Zeiser, M. Bogyo, V. Turk, S.G. Psakhye, B. Turk and O. Vasiljeva, *Nat. Nanotechnol.*, 2011, **6**, 594-602.
4 S. Biswas, N.S. Dodwadkar, P.P. Deshpande and V.P. Torchilin, *J. Control. Release,* 2012, **159**, 393-402.
5 J. Mai, S. Song, M. Rui, D. Liu, Q. Ding, J. Peng and Y. Xu, *J. Control. Release,* 2009, **139**, 174-181.
6 V.P. Chekhonin, V.P. Baklaushev, G.M. Yusubalieva, A.E. Belorusova, M.V. Gulyaev, E.B. Tsitrin, N.F. Grinenko, O.I. Gurina and Y.A. Pirogov, *Nanomed-Nanotechnol.*, 2012, **8**, 63-70.
7 L.E. Paulis, I. Jacobs, N. Akker, T. Geelen, D. Molin, L.W. Starmans, K. Nicolay and G.J. Strijkers, *Nanobiotechnol.*, 2012, **10**, 1-12.
8 E. Cittadino, M. Ferraretto, E. Torres, A. Maiocchi, B.J. Crielaard, T. Lammers, G. Storm, S. Aime and E. Terreno, *Eur. J. Pharm. Sic.*, 2012, **45**, 436-441.
9 T.M. Allen and P.R. Cullis, *Adv. Drug Deliv. Rev.*, 2013, **65**, 36-48.
10 D. Kozlowska, P. Foran, P. MacMahon, M.J. Shelly, S. Eustace and R. O'Kennedy, *Adv. Drug Deliv. Rev.,* 2009, **61,** 1402-1411.
11 V.P. Torchilin, *Adv. Drug Deliv. Rev.*, 2012, **64**, 302-315.
12 Y. Katanasaka, T. Ishii, T. Asai, H. Naitou, N. Maeda, F. Koizumi, S. Miyagawa, N. Ohashi and N. Oku, *Int. J, Cancer*, 2010, **127**, 2685–2698.
13 A. Etzerodt, M.B. Maniecki, J.H. Graversen, H.J. Møller, V.P. Torchilin and S.K. Moestrup, *J. Control. Release,* 2012, **160**, 72-80.
14 S. Kaida, H. Cabral, M. Kumagai, A. Kishimura, Y. Terada, M. Sekino, I. Aoki, N. Nishiyama, T. Tani and K. Kataoka, *Cancer Res.,* 2010, **70**, 7031-7041.
15 P.G. Tardi, N.D. Santos, T.O. Harasym, S.A. Johnstone, N. Zisman, A.W. Tsang, D.G. Bermudes and L.D. Mayer, *Mol. Cancer Ther.,* 2009, **8**, 2266-2275.
16 Y. Liu, W.L. Lu, J. Guo, J. Du, T. Li, J.W. Wu, G.L. Wang, J.C. Wang, X. Zhang and Q. Zhang, *J. Control. Release,* 2008, **129**, 18-25.
17 S. Jain, V. Mishra, P. Singh, P.K. Dubey, D.K. Saraf and S.P. Vyas, *Int. J. Pharm.,* 2003, **261**, 43-55.
18 S. Koudelka and J.Turánek, *J. Control. Release,* 2012, **163**, 322-334.
19 K. Na, S.A. Lee, S.H. Jung and B.C. Shin, *Colloid. Surface. B.,* 2011, **84**, 82-87.
20 Y. Liu and N. Zhang, *Biomaterials,* 2012, **33**, 5363-5375.
21 M. Tan and Z. Lu, *Theranostics,* 2011, **1**, 83-101.
22 Z. Yang, S.G. Kang and R. Zhou, *Nanoscale*, 2014, **6**, 663-677.
23 D. Yoo, J.H. Lee, T.H. Shin and J. Cheon, *Acc. Chem. Res.,* 2011, **44**, 863–874.
24 C. Li, *Nat. Mater.*, 2014, **13**, 110-115.
25 Y.L. Wu, N. Putcha, K.W. Ng, D.T. Leong, C.T. Lim, S.C.J. Loo and X. Chen, *Acc. Chem. Res.*, 2013, **46**, 782–791.
26 J.S. Desgrosellier and D.A. Cheresh, *Nat. Rev. Cancer,* 2010, **10**, 9-22.
27 Y. Wang, K. Zhou, G. Huang, C. Hensley, X. Huang, X. Ma, T. Zhao, B.D. Sumer, R.J. DeBerardinis and J. Gao, *Nat. Mater.,* 2014, **13**, 204-212.

28 L. Zhao, Y.H. Xu, T. Akasaka, S. Abe, N. Komatsu, F. Watari and X. Chen, *Biomaterials*, 2014, **35**, 5393-5406.

29 X. Ma, J. Jia, R. Cao, X.Wang and H. Fei, *J. Am. Chem. Soc.,* 2014, **136**, 17734-17737.

30 M. Schottelius, B. Laufer, H. Kessler and H.J. Wester, *Acc. Chem. Res.,* 2009, **42**, 969-980.

31 G.K. Seward, Y. Bai, N.S. Khan and I.J. Dmochowski, *Chem. Sci.,* 2011, **2**, 1103-1110.

32 G.J. Strijkers, E. Kluza, G.A.F. Tilborg, D.W.J. Schaft, A.W. Griffioen, W.J.M. Mulder and K. Nicolay, *Angiogenesis,* 2010, **13**, 161-173.

33 R. Haubner, W.A. Weber, A.J. Beer, E. Vabuliene, D. Reim, M. Sarbia, K.F. Becker, M. Goebel, R. Hein, H.J. Wester, H. Kessler and M. Schwaiger, *PLOS Med.,* 2005, **2**, 0244-0252.

34 Y. Miura, T. Takenaka, K. Toh, S. Wu, H. Nishihara, M.R. Kano, Y. Ino, T. Nomoto, Y. Matsumoto, H. Koyama, H. Cabral, N. Nishiyama and K. Kataoka, *ACS NANO,* 2013, **7**, 8583-8592.

35 S. Xu, B.Z. Olenyuk, C.T. Okamoto and S.F.H. Alvarez, *Adv. Drug Deliv. Rev.,* 2013, **65**, 121-138.

36 Y. Yoshizawa, K. Ogawara, A. Fushimi, S. Abe, K. Ishikawa, T. Araki, G. Molema, T. Kimura and K. Higaki, *Mol. Pharm.,* 2012, **9**, 3486-3494.

37 J. Du, W.L. Lu, X. Ying, Y. Liu, P. Du, W. Tian, Y. Men, J. Guo, Y. Zhang, R.J. Li, J. Zhou, J.N. Lou, J.C. Wang, X. Zhang and Q. Zhang, *Mol. Pharm.,* 2009, **6**, 905-917.

38 V.P. Torchilin, *Nat. Rev.,* 2005, **4**, 145-160.

39 P. Crosasso, M. Ceruti, P. Brusa, S. Arpicco, F. Dosio and L. Cattel, *J. Control. Release,* 2000, **63**, 19-30.

40 M. Hossann, T. Wang, Z. Syunyaeva, M. Wiggenhorn, A. Zengerle, R.D. Issels, M. Reiser, L.H. Lindner and M. Peller, *J. Control. Release,* 2013, **166**, 22-29.

41 S. Meng, B. Su, W. Li, Y. Ding, L. Tang, W. Zhou, Y. Song, H. Li and C. Zhou, *Nanotechnology,* 2010, **21**, 1-7.

42 J.A. Zhang, G. Anyarambhatla, L. Ma, S. Ugwu, T. Xuan, T. Sardone and I. Ahmad, *Eur. J. Pharm. Biopharm.,* 2005, **59**, 177-187.

43 A. Sharma, E. Mayhew, L. Bolcsak, C. Cavanaugh, P. Harmon, A. Janoff and R.J. Bernacki, *Int. J. Cancer,* 1997, **71**, 103-107.

44 P. Ma and R.J. Mumper, *J. Nanomed. Nanotechol.*, 2013, **4**, 1-16.

45 V.P. Chauhan and R.K. Jain, *Nat. Mater*., 2013, **12**, 958-962.

Nanoscale Accepted Manuscript